Journal of Computational Physics **148,** 291–298 (1999)
Article ID jcph.1998.6111, available online at http://www.idealibrary.com on IDEAL®

NOTE

A Spline Collocation Scheme for the Spherical Shallow Water Equations

Key Words: numerical weather prediction; spherical PDEs; pole problem; reduced grid; method of lines.

1. INTRODUCTION

The shallow water equations describe large scale horizontal phenomena of the global atmospheric motion to good approximation. Thus they provide a widely accepted primary test for numerical methods for global atmospheric modelling before proceeding to complete 3D baroclinic models [7]. They are prognostic equations for the (horizontal) velocity field and the depth of a shallow homogeneous, incompressible, hydrostatic, and inviscid fluid layer on a rotating sphere.

Currently there is a controversy on the question which of the different approaches to the integration of global models is preferable. For example, the European Centre for Medium Range Weather Forecasts (ECMWF) and the National Center for Atmospheric Research (NCAR) run spectral transform methods, which use spherical harmonics for the spatial discretization, whereas currently at German Weather Service (DWD) a finite difference scheme on a uniform triangular grid is developed. Although spectral methods are superior at today's resolutions, it seems that grid point schemes will be competitive in the future, since they allow for adaptivity and they appear more appropriate for massively parallel computer systems. In this research note we present a spline collocation scheme for the shallow water equations, a preliminary version of which already has been studied in detail for the scalar advection equation in [1, 2].

Let $\Omega := \{(x, y, z) \in \mathbb{R}^3, x^2 + y^2 + z^2 = 1\}$ for the two-dimensional unit sphere. From a theoretical point of view it is convenient to formulate spherical differential equations coordinate-free. But for the parametrization of partial differential operators and vector fields on the sphere we need local coordinates. We will use standard polar coordinates $(\lambda, \vartheta) \in [0, 2\pi] \times [-\pi/2, \pi/2]$ on the strip $\{(x, y, z) \in \Omega, |z| \le 1/\sqrt{2}\}$ around the equator and two stereographic coordinate systems $(\xi, \eta) \in \mathbb{R}^3$ on the polar caps $\{(x, y, z) \in \Omega, z \ge 1/\sqrt{2}\}$ and $\{(x, y, z) \in \Omega, z \le -1/\sqrt{2}\}$. Of course, this particular partition is somewhat

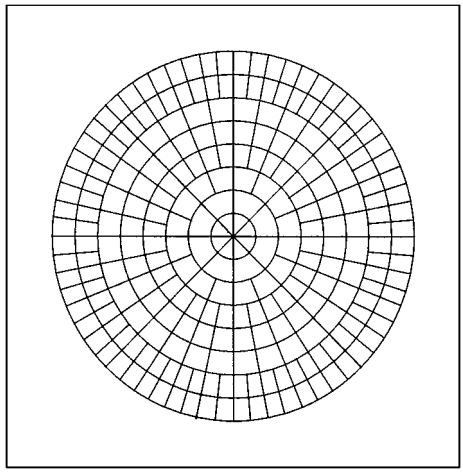

FIG. 1. The polar region of the reduced grid $\mathcal{T}_4$.

arbitrary, but it is irrelevant to the following. We will write $\mathbf{v} := (u, v, 0)$ for horizontal velocity fields, where u and v are the velocity components in λ- and ϑ-directions (or in ξ- and η-directions), respectively.

Now we briefly sketch a construction [1, 2] of spherical splines on a reduced grid. Therefore, let $\Delta\vartheta^{(j)} := \pi/2^{j+1}$ and $\Delta\lambda_k^{(j)} := 2^{r_k^{(j)}}(\pi/2^{j+1})$ for $k = 0(1)2^{j+1}$, where

$$r_k^{(j)} := \begin{cases} j+2 & \text{for } k = 0 \text{ or } k = 2^{j+1}, \\ \lfloor j + 1 - \ln_2(\pi k) \rfloor & \text{for } 0 < k < 2^{j-1}, \\ 0 & \text{for } 2^{j-1} \le k \le 3 \times 2^{j-1}, \\ \lfloor j + 1 - \ln_2(\pi(2^{j+1} - k)) \rfloor & \text{for } 3 \times 2^{j-1} < k < 2^{j+1}, \end{cases} \tag{1}$$

and let $K_j := \{(i,k), k = 0(1)2^{j+1}, i = 0(2^{r_k^{(j)}})2^{j+2} - 2^{r_k^{(j)}}\}$. With grid points $\omega_{(i,k)}^{(j)} := (\lambda_i^{(j)}, \vartheta_k^{(j)}) := (i\Delta\lambda_k^{(j)}, -\pi/2 + k\Delta\vartheta^{(j)})$, reduced grids are defined by $\mathcal{T}_j := \{\omega_{(i,k)}^{(j)}, (i,k) \in K_j\}$ (see Fig. 1). They are constructed from the equiangular standard grids (corresponding to $r_k^{(j)} \equiv 0$) by dropping grid points close to the poles. By this procedure the pole problem is eliminated. Let $\Delta x_j^{\min}$ and $\Delta x_j^{\max}$ be the minimal and maximal distances between neighbours in $\mathcal{T}_j$, respectively. Then for $r_k^{(j)}$ as defined in (1) there holds $\Delta x_j^{\max} \simeq \Delta x_j^{\min} \simeq 2^{-j}$; see also Table I. Piecewise bilinear splines adopted to $\mathcal{T}_j$ are

TABLE I

Characteristics of the Reduced Grids and Diffusion Constants

Level of resolution j	Corresp. spectral truncation TN	$\Delta x_j^{\max}$	$\Delta x_j^{\min}$	$\dim V_j = \lvert\mathcal{T}_j\rvert$	Diffusion constant κ
3	T10	1251 km	694 km	482	$1.0 \cdot 10^{-5}$
4	T21	626 km	347 km	1986	$3.0 \cdot 10^{-7}$
5	T42	313 km	161 km	8066	$3.0 \cdot 10^{-8}$
6	T85	156 km	77 km	25714	$2.0 \cdot 10^{-9}$

defined by

$$\varphi_{(i,k)}^{(j)}(\lambda,\vartheta) := \begin{cases} \max\left\{0, 1-\frac{|\vartheta_k^{(j)}-\vartheta|}{\Delta\vartheta^{(j)}}\right\} & \text{for } k = 0, 2^{j+1}, \\ \max\left\{0, 1-\frac{|\lambda_i^{(j)}-\lambda|}{\Delta\lambda_k^{(j)}}\right\} \cdot \max\left\{0, 1-\frac{|\vartheta_k^{(j)}-\vartheta|}{\Delta\vartheta^{(j)}}\right\} & \text{for } k = 1(1)2^{j+1}-1, \end{cases} \tag{2}$$

and $V_j := \operatorname{span}\{\varphi_{(i,k)}^{(j)}, (i,k) \in K_j\}$. Finally let $\tilde{\varphi}_{(i,k)}^{(j)} := \delta(\cdot - \omega_{(i,k)}^{(j)})$ the Dirac functional centered at $\omega_{(i,k)}^{(j)} \in \Omega$. Obviously there holds are biorthogonality relation,

$$\left(\tilde{\varphi}_{(i',k')}^{(j)}, \varphi_{(i,k)}^{(j)}\right) = \delta_{(i',k'),(i,k)}. \tag{3}$$

2. DISCRETIZATION OF THE SHALLOW WATER EQUATIONS

For the derivation of the shallow water equations we refer to the literature [3]. In nondimensional variables and in coordinate-free form, the equations of motion and continuity are written as

$$\frac{\partial \mathbf{v}}{\partial t} + \mathbf{v}\cdot\nabla\mathbf{v} = f\mathbf{v}\times\mathbf{k} - \nabla h, \quad \frac{\partial h}{\partial t} + \mathbf{v}\cdot\nabla(h-h_s) = -(h-h_s)\nabla\cdot\mathbf{v}. \tag{4}$$

Here h is the depth of the fluid, h_s is the height of the underlying topography, $\mathbf{v}$ is the horizontal velocity field, f is the Coriolis parameter, and $\mathbf{k}$ is the outer unit normal vector. We applied the scaling $h \mapsto ((2\phi a)^2/g)h$, $\mathbf{v} \mapsto 2\phi a\mathbf{v}$, and $t \mapsto t/2\phi$ with g the constant of gravity, a the earth's radius, and ϕ its angular velocity. For the discretization we rewrite the equations in local coordinates. For example, in polar coordinates the equation of continuity reads

$$\frac{\partial h}{\partial t} + \frac{u}{\cos\vartheta}\frac{\partial(h-h_s)}{\partial\lambda} + v\frac{\partial(h-h_s)}{\partial\vartheta} = -\frac{(h-h_s)}{\cos\vartheta}\left(\frac{\partial u}{\partial\lambda} + \frac{\partial\cos\vartheta\, v}{\partial\vartheta}\right). \tag{5}$$

Now assume we are given initial values $h(0) = h_0$ and $\mathbf{v}(0) = \mathbf{v}_0$. For the evolution in time we discretize the system separately in space and in time, following the method of lines. Substituting the approximations

$$h(t) \approx \sum_{(i,k)\in K_j} h_{(j,(i,k))}(t)\varphi_{(i,k)}^{(j)}, \quad \mathbf{v}(t) \approx \sum_{(i,k)\in K_j} \left(u_{(j,(i,k))}(t), v_{(j,(i,k))}(t), 0\right)\varphi_{(i,k)}^{(j)} \tag{6}$$

in the continuous equations (4) and applying the biorthogonal Dirac functionals to any component yields a system of ordinary differential equations for the unknown continuous time coefficients. Now we exploit the biorthogonality relation (3) and the fact that

$$\left(\tilde{\varphi}_{(i,k)}^{(j)}, fg\right) = \left(\tilde{\varphi}_{(i,k)}^{(j)}, f\right)\left(\tilde{\varphi}_{(i,k)}^{(j)}, g\right) \tag{7}$$

for any functions $f, g : \Omega \to \mathbb{R}$. For the full discretization we fix time steps $\Delta t_j^{(n)}$ and approximate the partial time derivatives at time $t_j^{(n)} := \sum_{n'=0}^{n-1} \Delta t^{(n')}$ by generalized centered

differences, involving the unknown variables at times $t_j^{(n+1)}$ and $t_j^{(n-1)}$ and evaluating the right-hand sides at time $t_j^{(n)}$. This yields approximations

$$\begin{aligned} h\big(t_j^{(n)}\big) &\approx h_j^{(n)} := \sum_{(i,k)\in K_j} h^{(n)}_{(j,(i,k))}\varphi^{(j)}_{(i,k)}, \\ \mathbf{v}\big(t_j^{(n)}\big) &\approx \mathbf{v}_j^{(n)} := \sum_{(i,k)\in K_j} \big(u^{(n)}_{(j,(i,k))}, v^{(n)}_{(j,(i,k))}, 0\big)\varphi^{(j)}_{(i,k)}. \end{aligned} \tag{8}$$

For example, from Eq. (5) the discrete time coefficients in the polar coordinate representation are calculated by

$$\begin{aligned} h^{(n+1)}_{(j,(i',k'))} = h^{(n-1)}_{(j,(i',k'))} &- \big(\Delta t_j^{(n)} + \Delta t_j^{(n-1)}\big) \\ &\times \Bigg[\frac{u^{(n)}_{(j,(i',k'))}}{\cos\vartheta^{(j)}_{k'}} \sum_{(i,k)\in K_j} \Gamma^{(1)}_{j,(i',k'),(i,k)} \big(h^{(n)}_{(j,(i,k))} - h_{s,(j,(i,k))}\big) \\ &+ \big(h^{(n)}_{(j,(i',k'))} - h_{s,(j,(i',k'))}\big) \sum_{(i,k)\in K_j} \Gamma^{(1)}_{j,(i',k'),(i,k)} \frac{u^{(n)}_{(j,(i,k))}}{\cos\vartheta^{(j)}_{k'}} \\ &+ v^{(n)}_{(j,(i',k'))} \sum_{(i,k)\in K_j} \Gamma^{(2)}_{j,(i',k'),(i,k)} \big(h^{(n)}_{(j,(i,k))} - h_{s,(j,(i,k))}\big) \\ &+ \big(h^{(n)}_{(j,(i',k'))} - h_{s,(j,(i',k'))}\big) \sum_{(i,k)\in K_j} \Gamma^{(2)}_{j,(i',k'),(i,k)} v^{(n)}_{(j,(i,k))} \\ &- \tan\vartheta^{(j)}_{k'} \big(h^{(n)}_{(j,(i',k'))} - h_{s,(j,(i',k'))}\big) v^{(n)}_{(j,(i',k'))} \Bigg] \end{aligned} \tag{9}$$

with the interaction coefficients

$$\Gamma^{(1)}_{j,(i',k'),(i,k)} := \left(\tilde\varphi^{(j)}_{(i',k')}, \frac{\partial\varphi^{(j)}_{(i,k)}}{\partial\lambda}\right), \quad \Gamma^{(2)}_{j,(i',k'),(i,k)} := \left(\tilde\varphi^{(j)}_{(i',k')}, \frac{\partial\varphi^{(j)}_{(i,k)}}{\partial\vartheta}\right). \tag{10}$$

Similar equations are derived from the equation of motion for $u^{(n+1)}_{(j,(i',k'))}$ and $v^{(n+1)}_{(j,(i',k'))}$ and for the stereographic coordinate representation, now involving the interaction coefficients

$$\Gamma^{(1)}_{j,(i',k'),(i,k)} := \left(\tilde\varphi^{(j)}_{(i',k')}, \frac{\partial\varphi^{(j)}_{(i,k)}}{\partial\xi}\right), \quad \Gamma^{(2)}_{j,(i',k'),(i,k)} := \left(\tilde\varphi^{(j)}_{(i',k')}, \frac{\partial\varphi^{(j)}_{(i,k)}}{\partial\eta}\right). \tag{11}$$

These coefficients are independent of time. Hence, they can be precalculated and stored, and the time-marching procedure reduces to simple matrix–vector multiplications. Since the trial functions $\varphi^{(j)}_{(i,k)}$ are not continuously differentiable, the partial derivatives in (10) and (11) cannot be taken in a classical sense. Essentially we replace them by centered differentials; thus we can consider the present method as a generalization of the classical leap-frog scheme. But to guarantee linear stability, we have to make modifications at those grid points $\omega^{(j)}_{(i',k')}$, where a change in the meridional stretching factor $r_k^{(j)}$ occurs. A detailed description is given in [1, 2].

2.1. Remark. Due to the biorthogonality of the trial functions and the test functionals no linear systems have to be inverted, and by (7) the quadratic nonlinearities in the continuous equations are discretized by simple sums. In total, to perform one time step we only have to index, read, and multiply approximately 300 N_j interaction coefficients, where $N_j := |\mathcal{T}_j| = dim\, V_j$.

To satisfy the linear stability criterion, the time steps are chosen according to the Courant–Friedrich–Lewy condition

$$\Delta t_j^{(n)} := \frac{\Delta x_j^{\min}}{2\left(|\mathbf{v}_j^{(n)}| + |h_j^{(n)}|^{1/2}\right)_{\ell^\infty(\mathcal{T}_j)}}. \tag{12}$$

In order to damp noise and to deal with the spectral blocking near the truncation limit, an explicit diffusion term is included. After every time step we correct any approximated variable z by $z - \kappa(2 - \sin\vartheta)\Delta^2 z$, where Δ is the Laplacian, discretized by the standard five-point stencil and adapted to the reduced grid, and $\kappa > 0$ is a constant (see Table I). The weight $2 - \cos\vartheta$ is introduced to compensate the irregular grid structure close to the poles.

3. NUMERICAL RESULTS

We applied the scheme to the complete standard test set for the spherical shallow water equations [7]. Here we only present and analyze some selected typical results; for more details we refer to [2]. As confirmed by the test cases 1 to 3, the poles are not exceptional points in our approach. For the scalar advection equation (test case 1) we could prove first-order consistency in space, second-order consistency in time, and conditional linear stability; hence, the method is convergent under the CFL condition. As expected, we observe numerical dispersion which is typical for centered difference approximations [3]. Numerical experiments confirmed these properties also for the nonlinear shallow water system.

3.1. EXAMPLE (Test case 5: zonal flow over an isolated mountain). This test consists of a zonal flow impinging on an isolated mountain which is centered at $(\lambda_c, \vartheta_c) = (3\pi/2, \pi/6)$ (for more details we refer to [7]). It describes the rapid evolution from a meridionally smooth symmetric flow to an irregular high wave number state. This test is designed to study the influence of nonflat topography and the conservation of integral invariants.

We observe convergence of the approximations (see Table II), where the error is calculated with respect to a reference solution in T213 resolution as described in [7]. Mass and energy are almost perfectly conserved. For comparison we show the errors for the spectral method [4, 5] with T42 and T63 resolution, which are of the same order. There is no marked influence of the irregular grid structure on the approximations (see Fig. 2) and in contrast to the spectral method there are no problems in the vicinity of the mountain; in particular we do not observe any "spectral ringing."

3.2. EXAMPLE (Test case 7: analyzed 500 mb height and wind field). This test consists of the atmospheric initial conditions of the 500 mb height and winds for January 16, 1979, initialized by nonlinear normal mode initialization [3, 4]. It is characterized initially by two cutoff lows, and the flow develops into a typical blocking situation. The mean height of the height field is set to 10 km, and we assume flat topography ($h_s = 0$).

TABLE II
Errors after 10 Days for Test Case 5 for Different Resolutions j

Level j	Time step Δt_j	Relative L^∞-error	Relative L^2-error	Normalized mass	Normalized energy
3	1500 s	4.97%	1.25%	0.998	0.989
4	750 s	4.07%	0.63%	1.000	0.997
5	360 s	1.22%	0.23%	1.000	0.999
6	180 s	0.30%	0.06%	1.000	1.000
T42	1200 s	1.40%	0.12%	1.000	1.000
T63	900 s	0.65%	0.12%	1.000	1.000

Note. The results for the spectral method with T42 and T63 truncation are estimated from [4, 5].

Table III shows qualitatively the same results as for test case 5. After five days of simulation the global structure of the height fields is well reproduced. But some small-scale details are slightly blurred, in particular in the northern hemisphere (see Fig. 3). We mention that plotting traces of the height field indicates some very weak presence of temporal noise or residual gravity waves, but this does not disturb the overall structure.

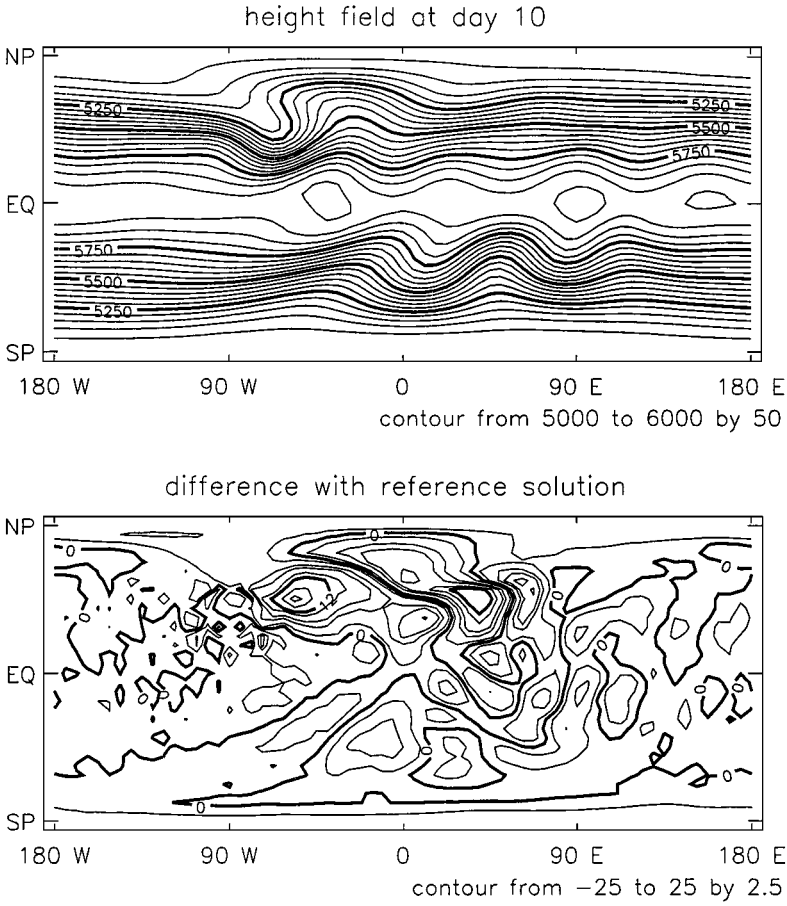

FIG. 2. The calculated height field and the difference with the reference solution at day 10 for test case 5 and $j = 6$.

TABLE III
As Table II after 5 Days for Test Case 7 (January 16, 1979)

Level j	Time step Δt_j	Relative L^∞-error	Relative L^2-error	Normalized mass	Normalized energy
3	1200 s	7.72%	1.68%	1.003	0.983
4	540 s	4.90%	0.78%	1.000	0.988
5	270 s	3.94%	0.58%	1.000	0.992
6	120 s	2.20%	0.38%	1.000	0.997
T42	1200 s	4.25%	0.53%	1.000	0.998
T63	900 s	2.00%	0.23%	1.000	0.999

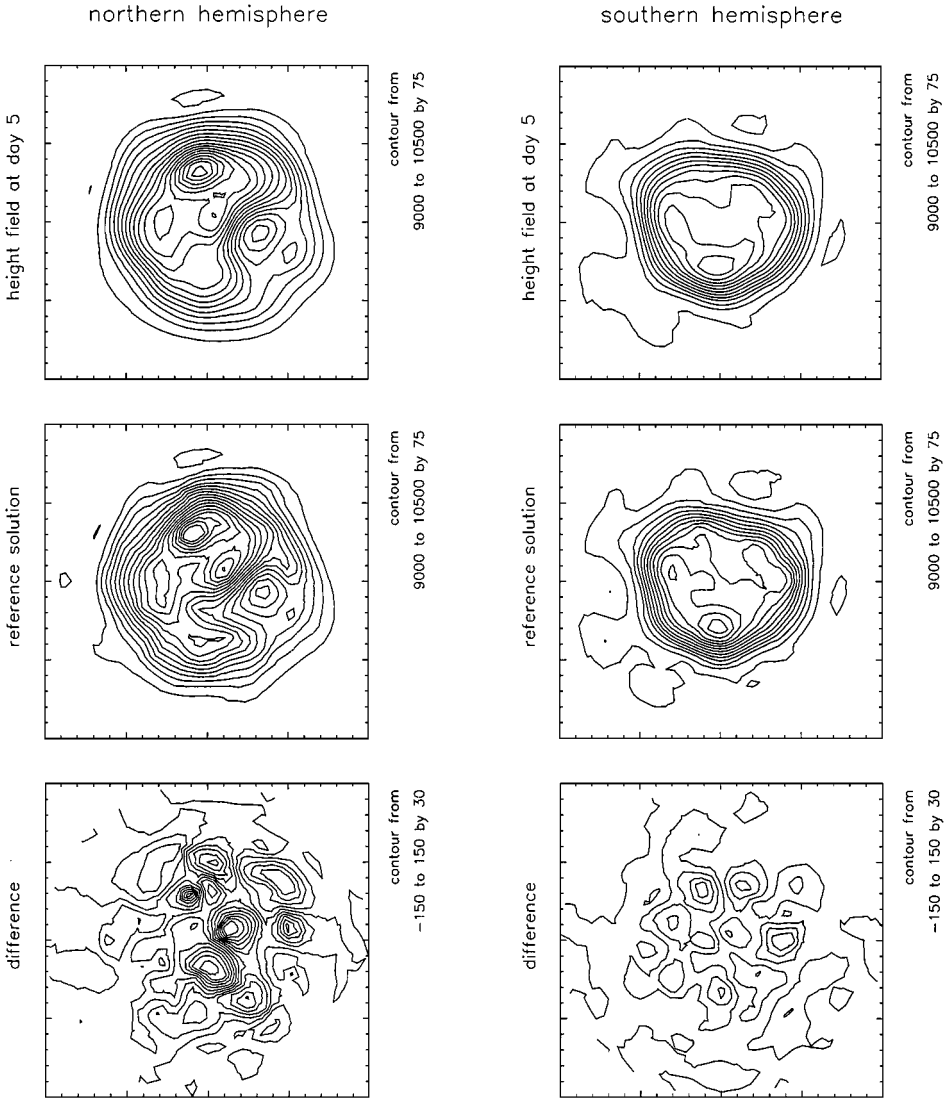

FIG. 3. Stereographic projections of the calculated height field, the reference solution, and the difference after 5 days for test case 7 (January 16, 1979) and $j = 6$.

4. CONCLUSIONS

A spline collocation scheme on a reduced spherical grid is formulated and applied to a standard benchmark test set. No special treatment at the poles is required. Although the spatial discretization is only of first order, numerical experiments show that at comparable resolutions it is as accurate as an established spectral method. Furthermore, nonflat topography does not cause any problems, and there are no spurious oscillations caused by Gibbs' phenomena.

By Remark 2.1, every time step in the time-marching procedure can be performed very efficiently. The price we have to pay is the very restrictive condition (12) on the time steps, since it is controlled by fast gravity waves, which represent noise within the shallow water model. This limits the overall efficiency of the method. In fact, there are semi-implicit semi-Lagrangian schemes which allow for time steps up to 2 h at resolutions even higher than $j = 6$. However, it is the best we can expect for a fully explicit method unless the gravity and Coriolis terms are treated implicitly. Since in this note we mainly focus on the spatial discretization, here we do not address the question of improved time integration schemes. Finally we mention that in principle it is possible to construct smoother trial functions on the reduced grids. This allows for higher order spatial discretizations.

Very currently the scheme has been reformulated as a biorthogonal wavelet scheme. The spatial domain can be resolved adaptively according to the structure of the solution or the topography. For the scalar advection equation this is discussed in detail in [1, 2]. First results on the shallow water equations can be found in [2] and will be published in a forthcoming paper.

ACKNOWLEDGMENT

I thank the anonymous referees for their valuable comments and suggestions.

REFERENCES

1. J. Göttelmann, An adaptive multiscale algorithm for the spherical advection equation, Preprint No. 8-97, Dept. of Mathematics, Univ. Mainz, Germany. [Submitted for publication]
2. J. Göttelmann, *Construction of Splines and Wavelets on the Sphere and Numerical Solutions to the Shallow Water Equations of Global Atmospheric Dynamics* (Logos Verlag, Berlin, 1998).
3. G. J. Haltiner and R. T. Williams, *Numerical Prediction and Dynamic Meteorology* (Wiley, New York, 1980).
4. R. Jakob, J. J. Hack, and D. L. Williamson, *Solutions to the Shallow Water Test Set Using the Spectral Transform Method*, Technical Note NCAR/TN-388+STR, NCAR, Boulder, CO, 1993).
5. R. Jakob-Chien, J. J. Hack, and D. L. Williamson, Spectral transform solutions to the shallow water test set, *J. Comput. Phys.* **119**, 164 (1995).
6. D. L. Williamson, Review of numerical approaches for modelling global transport, in *Air Pollution Modelling and its Applications*, edited by H. van Dop and G. Kallos (Plenum, New York, 1992).
7. D. L. Williamson, J. B. Drake, J. J. Hack, R. Jakob, and P. N. Swarztrauber, A standard test set for numerical approximations to the shallow water equations in spherical geometry. *J. Comput. Phys.* **102**, 211 (1992).

Received March 3, 1998; revised September 9, 1998

Jochen Göttelmann
Johannes Gutenberg University,
55099 Mainz,
Germany
E-mail: jochen@mat.mathematik.uni-mainz.de